Journal of the Korean Physical Society, Vol. 49, No. 4, October 2006, pp. 1652∼1666

# A Stochastic Model of Cancer Growth with Immune Response

A. Boondirek and Y. Lenbury
*Department of Mathematics, Faculty of Science, Mahidol University, Bangkok 10400, Thailand*

J. Wong-ekkabut
*Department of Physics, Faculty of Science, Mahidol University, Bangkok 10400, Thailand*

W. Triampo*
*Capability Building Unit in Nanoscience and Nanotechnology, Faculty of Science, Mahidol University, Bangkok, 10400, Thailand*

I. M. Tang
*Institute of Science and Technology for Research and Development, Mahidol University, Nakhonpathom 73170, Thailand*

P. Picha
*National Cancer Institute of Thailand, Bangkok 10400, Thailand*

(Received 1 April 2006, in final form 12 July 2006)

A cellular automaton model for the growth of an avascular tumor on a two-dimensional square lattice is presented. The pattern formation and the growth of the cell population are investigated by using a Monte Carlo simulation. A microscopic description of the immune system response, including cell proliferation, cell death, and cell degradation, is used to simulate the growth. In particular, the escape rate for cancer from immune surveillance is included for consistency with experimental observations. The simulation results give rise to a growth curve with an explanation on a microscopic scale that is shown to agree well with experimental animal tumor growth and relevant biological implications. Our model clearly shows that an increase in the lysis rate leads to a decrease in the proliferation rate of cancer cells. The spatial distribution of proliferated cell and the fractal dimension of the boundary are also measured.

PACS numbers: 87.15.Aa, 87.17.Aa
Keywords: Cancer growth, Immune response, Cellular automaton, Monte Carlo, Gompertz curve

## I. INTRODUCTION

Cancer has been a leading cause of human death in the world. There is not too much known about the biological mechanisms leading to the establishment of or the growth of malignant tumors. Many attempts have been made in recent decades to describe the basic biological mechanisms of tumor growth.

Most tumor growth models were proposed to investigate one or several basic features, such as the cell cycle, the cell proliferation, the lack of nutrients, the competition for resources, and the cytotoxic activity by the immune response [1–29]. Two types of approaches have been used to describe the growth of the tumor: the continuous models [17, 30] and discrete models [1–4, 8, 15, 22, 27–29, 31]. A few discrete models have used an automaton-based method. These cellular automaton (CA) models are based on the properties of the actual cells at the cellular level, that is, the microscopic scale. The CA models use microscopic-scale information to determine the cellular automata rules by applying the rules for each time step in an iterative manner. In this way, the CA models, which use the Monte Carlo approach to the cell dynamics, might be called Monte Carlo Cellular Automaton models. This approach is also well known to be very useful for a myriad of stochastic process applications [32,33].

One of the cancer growth modelling aspects is the immune response. However, the precise natural complexity of the immune response remains poorly understood. Many studies have established that the immune response plays a crucial role in eliminating cancer cells from healthy tissues [23,26,34–37]. A number of authors [23,26], Bell [35–37] have focused on the details at the cellular level of immune cell binding and delivery of lethal

*E-mail: scwtr@mahidol.ac.th; Fax: +66-2-201-5843

hits. In particular, in 1984 Lefever and Erneaux [23] proposed a reaction diffusion formulation of the growth of cancerous tissue attacked by immune cytotoxic cells they used a system of kinetic equations for cell growth and cell-mediated cytolysis in tumors composed of a two-step reaction for the kinetics of cell-mediated cytolysis in tumors. This reaction led only to the tumor-immune cell complexes producing either dead tumor cells or immune cells.

In 1994, Kuznetsov and Taylor [21] proposed a new model for the tumor-immune interaction, which included the two step reactions in Ref [23]. What was new in Kuznetsov and Taylor's model (KT model) was the detachment (or breaking up) of tumor-immune cell complexes from each other. The detachment of the complexes was assumed to occur without damaging the tumor cell, inactivating the immune cell, changing the programming for the lysis of tumor cell, or activating an immune cell to become cancerous. Several assumptions made by Kuznetsonov and Taylor [21] have lead several researchers, like Matzavinos and Chaplain [10,11] Galach [14] to develop new models to investigate the dynamics of tumor-immune system competition.

Qi *et al.* [1]developed a cellular automaton model of cancerous growth with a microscopic description applying a system of kinetic equations for the growth and cell-mediated cytolysis in tumors proposed by Lefever and Erneaux [23] including the mechanical pressure arising from within the tumor [38]. They attempted to provide a microscopic explanation for the Gompertz growth by establishing a set of probabilistic cellular automaton (PCA) rules. Their simulated results produced a Gompertzian growth curve with a significant fluctuating component.

The major purpose of this research is to further develop the CA model of Qi *et al.* [1] to include more realistic biological implications from the KT model. In particular, we create a novel fundamental kinetics model of tumor growth while neglecting the behavior of the mechanical pressure. The new fundamental kinetics model is able to describe the interaction and the competition between the tumor and the immune system. Additionally, our model takes into account tumor-cell proliferation, the tumor's interaction with the immune system, resulting in either lysis of the proliferating tumor cells or the detachment of immune binding without damaging the cancer cells, as well as the removal of dead tumor cells in avascular tumors. By adding the detachment of immune binding without damaging cancer cells, we found a different result from Qi *et al.* [1] with regard to the variation of the lysis rate. A large lysis rate gives a lower number of proliferating cancer cells. This agree well, in particular, with the experimental results from hormonal therapy with tamoxifen [39, 40]. We have neglected the presence of inactivated tumor-infiltrating cytotoxic lymphocytes (TICLs), which are in the KT model. The Monte-Carlo approach employs the PCA rules, as in the models of Smolle and Stettner [4] and Conolly and Kimbell [27].

The paper is organized as follows: A phenomenological description of the tumor-immune interaction, and the method of the CA model are presented in Section II. In Section III, we present the simulation results for tumor progression. Then, insection IV, we compare the simulated results with the *in vivo* experimental results and find that the two are inagreement in many respects. For instance, the average growth curve of a thousand tumors simulated by our model agrees well with the Gompertzian growth curve of Ehrlich mouse carcinomas and spontaneous mouse carcinomas (C3H) as reported by Steel [41]. Also, the tumor morphology show that mainly proliferating cells are located at the outermost region of a tumor and that the fractality of the tumor boundaries agree well with the clinical experimental results of Bru *et al.* [20, 42]. A computational investigation was performed to determine the qualitative growth curves for the dynamics for various value of each parameter in a sensitivity analysis, as discussed in Section 4, and some biological implications are given. In Section 5, several conclusions and a discussion are given.

## II. OUTLINE OF THE CA MODEL

### 1. Model Design Rationale

It is well established that the immune system plays an important role in the growth of avascular tumors. Since the dynamics of the antitumor immune response *in vivo* is very complicated, following Matzavinos and Chaplain [10] we make a biological assumption about the tissue of a small multicellular tumor. The tumor-infiltrating cytotoxic lymphocytes (TICLs) have an element of random motility, so the kinetic model focuses on the attack on tumor cells by TICLs without necrosis and at the stage prior to (tumor-induced) angiogenesis.

According to the clinical studies in Matzavinos and Chaplain [10], "*the tumor development can be effectively eliminated by tumor-infiltrating cytotoxic lymphocytes (TICLs) during the avascular stage. The TICLs may be cytotoxic lymphocytes (CTLs, CD8$^+$ cells), natural killer-like (NK-like) cells, and/or lymphokine-activated killer (LAK) cells, including the cytostatic/cytotoxic activity of granulocytes and monocytes/macrophages lymphokine activated in the tumor.*" The TICLs can interact with the tumor cell, forming lymphocyte-tumor-cell complexes. The detachment results in the proliferating tumor cells dying due to programmed lysis or or escaping due to immune surveillance [10,44].

The escape mechanism that prevents the activation of the immune system has been studied by Anichini and Morarini [44]. One of the reasons for the escape result is that the cancer cells shed the antigen peptides on their surfaces, and by releasing blocking factors, which

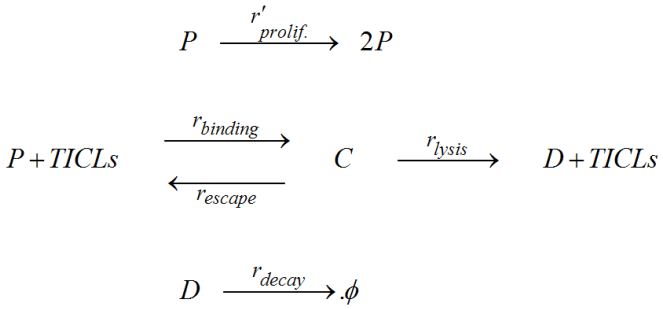


Fig. 1. Fundamental features of the development of cancer with an immune response (modified from Jain [37] and Matzavinos and Chaplain [10].

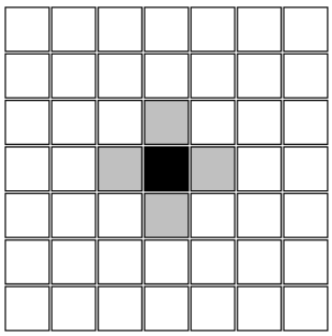

Fig. 2. Four nearest-neighboring sites (gray) of the tumor site (black) and the Nearest-neighbor rule (the so-called von *Neumann* neighborhoods).

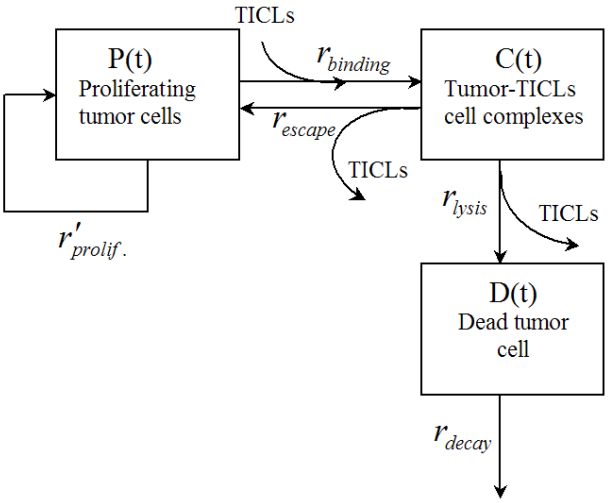


Fig. 3. Schematic diagram illustrating how cells in the tissue may change their state from one to another, and how cancer cells reproduce. $P(t)$ denotes the number of proliferating cells at time $t$, $C(t)$ denotes the number of TICLs-tumor cell complexes, and $D(t)$ denotes the number of dead tumor cells. In this model, the function $r'_{prolif.}$ depends on the number of proliferating cells and on the carrying capacity of the proliferating cells.

can neutralize NK cells [37], they can decrease the efficiency of cytotoxicity behavior of immune activations [34]. A decline of the proliferation rate with increasing proliferation-tumor-cell numbers is assumed in the case of avascular microscopic tumor growth *in vivo* [20, 34, 41, 44, 45]. We will address these facts as fundamental assumptions to the model.

## 2. Fundamental Feature of Cancer Development With an Immune Response

The mathematical function [1] $r'_{prolif.}(t) = r_{prolif.}\left(1-\frac{P}{K}\right)$, as an *in vivo* avascular tumor growth rate, where $P(t)$ is the number of proliferating tumor cells and $K$ is the carrying capacity for tumor proliferation, has been defined. Simply speaking, the proliferation rate includes the crowding effect of viable tumor cells. As is evident, $r'_{prolif.}$ decreases when there is an increase in the number of proliferating malignant tumor cells. This will affect the first output of the first reaction as shown in Fig. 1 or Fig. 3. Moreover, the parameter $r_{prolif.}$ could indicate the proliferative activity of tumor cells. The definition of the rate of avascular tumor growth *in vivo*, $r'_{prolif.}$, may arise from limitation on the amount of nutrient that is available for the proliferation of cancer cells or from increasing accumulation of waste products, which causes a decrease in the proliferation rate of cancer cells [20,44].

In the second reaction, which we may call the cytolysis reaction, the parameter $r_{binding}$ is a measure of the recognition or response of TICLs to the proliferating tumor cells. The parameter $r_{escape}$ describes the potential for the tumor escaping the host's immune surveillance [10,44]. The parameter $r_{lysis}$ describes the potential for the immune system to deliver lethal hits to a tumor cell or to program a tumor cell's death [10,23,26,27,35].

For the last reaction, we introduce the parameter rdecay $r_{decay}$, which describes dissolution or disappearance of the dead cancer cells from the tumor (although, there is no definitive experimental data on the details of this tumor-cell destruction, a few authors have used this parameter [1,4,14,23,26,28,37,41].

According to the description above we denote the proliferating tumor cells, the dead tumor cells, the tumor infiltrating cytotoxic lymphocytes and the TICLs-tumor cell complexes by $P$, $D$, $TICLs$, and $C$, respectively. The fundamentals of tumor development are schematically represented in Fig. 1.

The parameters $r_{prolif.}$, $r_{binding}$, $r_{escape}$, $r_{lysis}$, and $r_{decay}$ are non-negative kinetic constants. $r_{prolif.}$ is the constant proliferation rate of tumor cells. $r_{binding}$ is the constant binding rate of TICLs to tumor cells. $r_{escape}$ is the constant detachment rate of TICLs from cancer cells without damage to the cells. $r_{lysis}$ is the detachment rate of TICLs from dead tumor cells due to the irreversible

programming of the tumor cells for lysis. The parameter $r_{decay}$ is the constant decay rate of dead tumor cells.

### 3. Methodology of the Cellular Automata Model

The fundamental kinetics of tumor growth is transferred to the PCA rules in the same way as done by Qi *et al.* [1]. After setting of PCA rules, we use a computer program to implement the cell dynamics by using stochastic processes. A flowchart of the Monte Carlo simulation algorithm is given in Appendix A.

We now describe this automata-based model in more detail. The host tissue is represented as a lattice of size $L \times L$. In the tissue model, the coordinates $(x_n,\ y_n)$ with $n = 1, 2, 3, \cdots, L$ are designated by different values to indicate either normal cells, proliferating tumor cells, viable cells, cell complexes, or dead tumor cells. $L$ is chosen to be sufficiently large so that the tumor cells never reach the boundary of the lattice, and there is no finite-size effect.

Time increases in discrete steps with synchronous updating, implying that in each time step, any site can be updated only once. We distinguish each tumor cell according to two possible states:

[1 ] Proliferating state (*i.e.*, cancer or proliferating tumor cell, $P$), and

[2 ] non-proliferating state or stationary state (*i.e.*, $C$ and $D$).

Each simulated tumor progresses according to the following algorithm:

(I) At the initial time step, $t = 0$ we start with an initial configuration of five cancer cells located at the center of normal tissue as shown in Fig. 2.

(II) At each subsequent time step the rules of the cellular automaton are applied to each tumorous cell with the cells being randomly selected one by one with the same probability when the same cell type the same rates are used. A randomly selected cell will carry out one of the actions upon its state as shown in the schematic diagram, Fig. 3, as follows:

(1) Proliferating state: If the selected cell is a cancer cell, the cell has one of three possible actions with the function $r'_{prolif.}$ and the parameter $r_{binding}$. :

(i) The cancer cell may invade a normal cell with a probability $r'_{prolif.}$ if the cancer cell has at least one nearest-neighbor normal cell randomly chosen with the same probability,

(ii) The cancer cell is bound by TICLs with a probability $r_{binding}$,

(iii) The cancer cell may not change with a probability $1 - (r'_{prolif.} + r_{binding})$ or there is no nearest neighboring normal sites in the case of invasion (probability $r'_{prolif.}$).

(2) Stationary state: If the selected cell is in a non-proliferating state, which consists of dead cancer cells and TICL-tumor complex cells, which may be defined as cell complexes, it is a dead cancer cell or a TICL-tumor complex cell (now called a cell complex).

(2.1) The complexes: The cell may take one of three actions with parameters $r_{escape}$, $r_{binding}$, and $r_{lysis}$:

(i) The complexes revert to a cancer cell with a probability $r_{escape}$,

(ii) The complexes may lysis to a dead cancer cells with a probability $r_{lysis}$,

(iii) The complexes may not change state with a probability $1 - (r_{escape} + r_{lysis})$

(2.2) The dead cancer cell: The site occupied by this dead cell may take on one of two actions according to parameter $r_{decay}$:

(i) The site may be reoccupied by a normal cell with probability $r_{decay}$,

(ii) The cell may not change with probability $1 - r_{decay}$,

All cells are selected, as in a time step.

(III) The PCA' rules (step II) are then applied iteratively to each time step until we reach a designated maximum number of time steps.

A pseudo-random number ($r$) is a part of a sequence generated by using a seed number supplied with a value in the range $0 < r < 1$, The probabilities of various events are distributed in the interval 0 to 1. That is, the sum of the probabilities of actions in each cancer cell has to less than one. For implementation of the rules for cancer cells, the setting parameters have to satisfy $r_{prolif.} + r_{binding} \leq 1$. Also, the setting parameters concerning the TICL-tumor-cell complexes have to satisfy $r_{escape} + r_{lysis} \leq 1$.

## III. SIMULATED RESULTS AND DISCUSSION

We have written a program to carry out the instructions given in the flowchart in Appendix A. The total number of tumor cells present at time $t$ is denoted by $N(t)$, which is equal to the sum of $P(t)$, the number of proliferating tumor cells at time $t$, $C(t)$, the number of TICL-tumor cell complexes at time $t$, and $D(t)$, the number of dead tumor cells at time $t$; that is, $N(t) =$

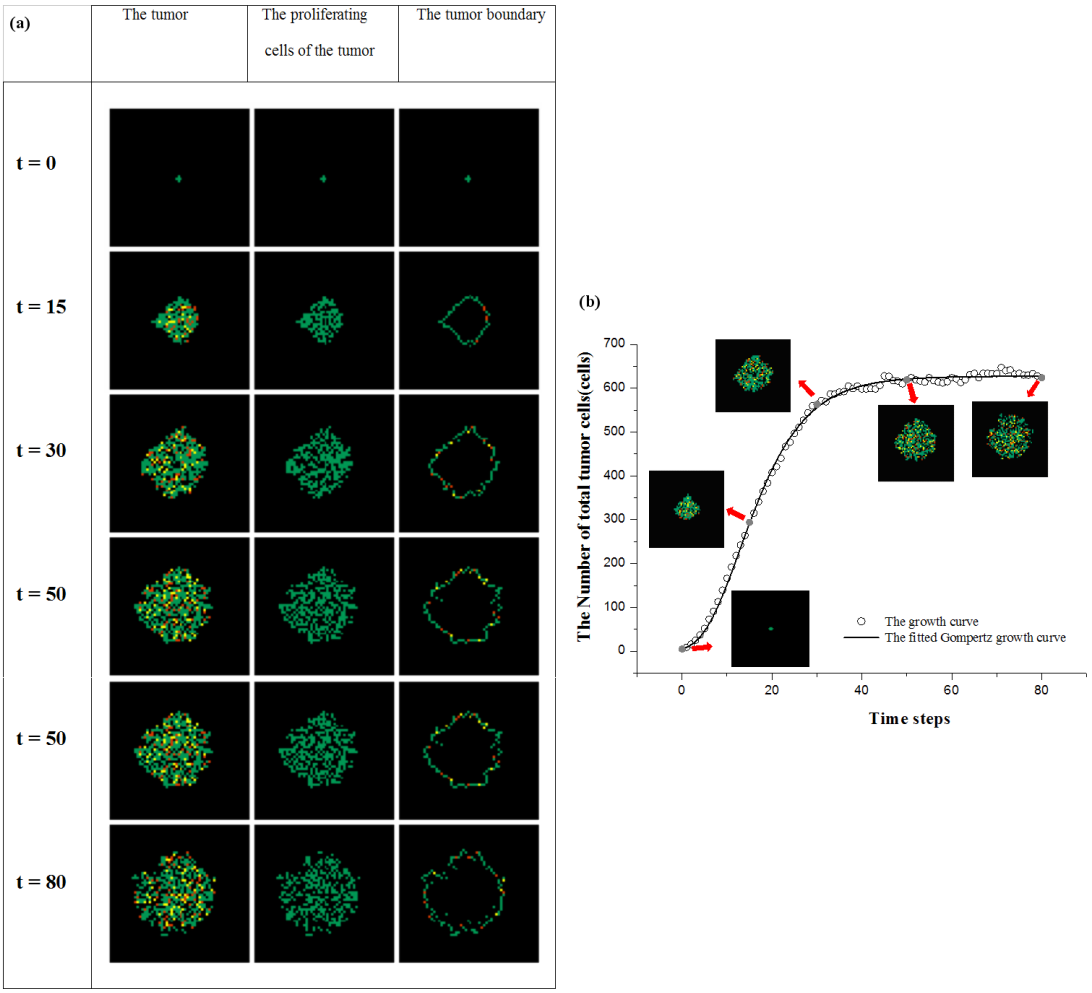


Fig. 4. (a) Snapshots of a simulated tumor on a $57 \times 57$ square lattice, the proliferating cell cluster and its boundary in time steps of 0,15, 30, 50, and 80, respectively. The simulation setting is $r_{prolif.} = 0.85$, $r_{binding} = 0.1$, $r_{escape} = 0.5$, $r_{lysis} = 0.35$, $r_{decay} = 0.35$, and $K = 550$. The color code is □: proliferating tumor cell, □: TICLs-tumor cell complexes, □: dead tumor cell, and □: normal cell. The definition of boundary cells for this model is a set of the outermost cells in each row and column of the two-dimensional square lattice. (b) Typical simulated tumor growth curve (circles) with the fitted Gompertz growth function. This fitting used the Gompertz parameters $A = 0.59363 \pm 0.00302$ and $B = 0.12285 \pm 0.00067$ with $r^2 = 0.99838$. This is the same simulation as in Fig. 4(a). The five snapshots of the simulated tumor at time steps of 0, 15, 30, 50, and 80 (solid gray) show the progression of the tumor shape.

$P(t)+C(t)+D(t)$. Consequently, $N(t)$ is the total number of tumor cells within a tumor, a measure of the size of the tumor at time $t$. We then average $N(t)$ over $Ts$ tumors, where $N(t)$ is the total number of tumor cells in the tumor, and $Ts$ is the number of tumors that are simulation.

The simulation is started by placing five tumor cells in the center of a square lattice. We then start the invasion of the tumor cells into the rest of the lattice, which represents normal tissue, by following the steps given in the algorithm of Section II.3. During a time step, we use a random number generator to choose the action that is to be taken by the cell, as detailed in Fig. 3. After a time step, the simulated results are obtained and a snapshot of the simulated tumor pattern at time $t$, as shown in Fig. 4(a). Several two-dimensional illustrations of tumor invasion into normal, tissue as generated by the program, are shown in Figs. 4(a), 4(b), and 6(a).

### 1. Snapshots of a tumor and Its Growth Curve: Gompertz Growth Function

Some typical snapshots of the simulated tumor generated at different times are seen in Fig. 4(a). Fig. 4(b) shows the growth curve of this tumor growth with a fitted Gompertz function. The proliferation function of tumor cells and the related growth curve are shown in Fig. 5(a). The growth curves of tumors are shown, to-

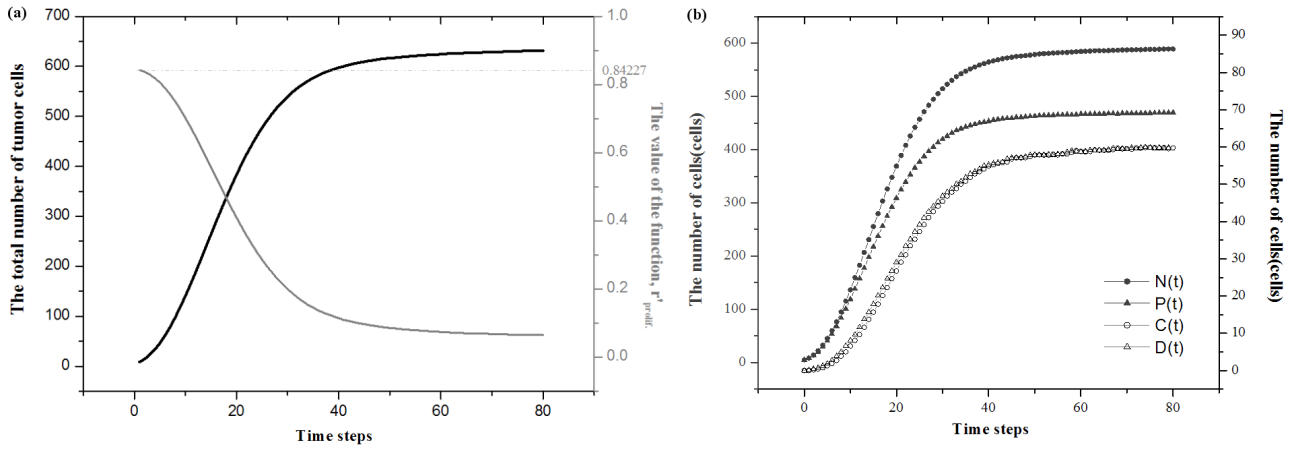


Fig. 5. (a) Plots of time evolutions of both the proliferating function value of avascular tumor growth, $r'_{prolif.}$ (gray solid line) and the total number of tumor cells (black solid line) from averaging 1000 simulated tumors. The proliferation rate of tumor cells *in vivo* is defined by $r'_{prolif.} = r_{prolif.}\left(1 - \frac{P}{K}\right)$, when $P$ is the number of proliferating cells in the tumor, and $K$ is the carrying capacity of the proliferating cells. We use the right axis for the functional value of $r'_{prolif.}$ and the left axis for the total number of tumor cells. The parameter settings are the same as in Fig. 4(a). (b) Time evolutions of the total number of tumor cells (gray solid circles), the number of proliferating cells (gray solid triangles), and the number of TICLs-tumor cell complexes (black triangles) and dead tumor cells (black stars). The averaged 1000 individual simulations use the same parameters as in Fig. 4(a).

Table 1. Summary of functions and constant input parameters for the model.

| | |
|---|---|
| Function in the model | |
| $r'_{prolif.}$ | Rate of proliferation of cancer cells (varies with the number of proliferating tumor cells) |
| Parameters | |
| $r_{prolif.}$ | Base rate of proliferation of cancer cells |
| $r_{binding}$ | Rate of TICLs binding with tumor cells form cell complexes |
| $r_{escape}$ | Rate of breaking TICLs detachment from complex cells without damaging tumor cells |
| $r_{lysis}$ | Rate of TICLs detachment from the complex cells as a result of the lysis of tumor cells |
| $r_{decay}$ | Rate of dead tumor cells being degraded to normal cells |
| $K$ | The carrying capacity of tumor proliferation |

∗ More extensive discussions of the parameters $r_{prolif.}$, $r_{binding}$, $r_{lysis}$, and $r_{decay}$ are given by Lefever and Erneaux [23] and Qi *et al.* [1] while more extensive discussions of $r_{escape}$ and $r_{lysis}$ are given by Matzavinos and Chaplain [10]. The experimental data of $r_{binding}$ and $r_{lysis}$ are given in Lefever and Erneux [59].

Table 2. Fitted Gompertz function fit to the growth curves of $P(t)$, $C(t)$, and $D(t)$ of Fig. 5(b).

| The type of cell in the tumor | $A$ | $B$ | Initial number of cells | Maximum number of cells | $r^2$ |
|---|---|---|---|---|---|
| Proliferating cell | 0.54588 | 0.00106 | 5 | 469.697 | 0.99977 |
| TICLs-cancer cell complexes | 0.50530 | 0.10538 | 0.493 | 59.755 | 0.99969 |
| Dead tumor cells | 0.58502 | 0.10023 | 0.175 | 59.913 | 0.99948 |

gether with their constituent parts (proliferating cells, cells complexes, and dead tumor cells), in Fig. 5(b).

## 2. Growth Fraction Function and Growth Curve

The proliferation rate *in vivo*, $r'_{prolif.}$, is the rate function due to the number of proliferating tumor cells in each time step, as represented in Fig. 5 for the same parameter settings as Fig. 4(a). Fig. 5(a) shows the time evolutions of the total number of tumor cells (black solid line; left axis) and the evolution of $r'_{prolif.}$ (gray solid line, right axis). The rate $r'_{prolif.}$ gives the same behavior as reported by Gyllenberg and Webb [31]. Their was a function of the total number of tumor cells, but $r'_{prolif.}$ in our model is a function of the ratio of the number of proliferating cells to the total number of tumor cells. The growth fraction with the same trend

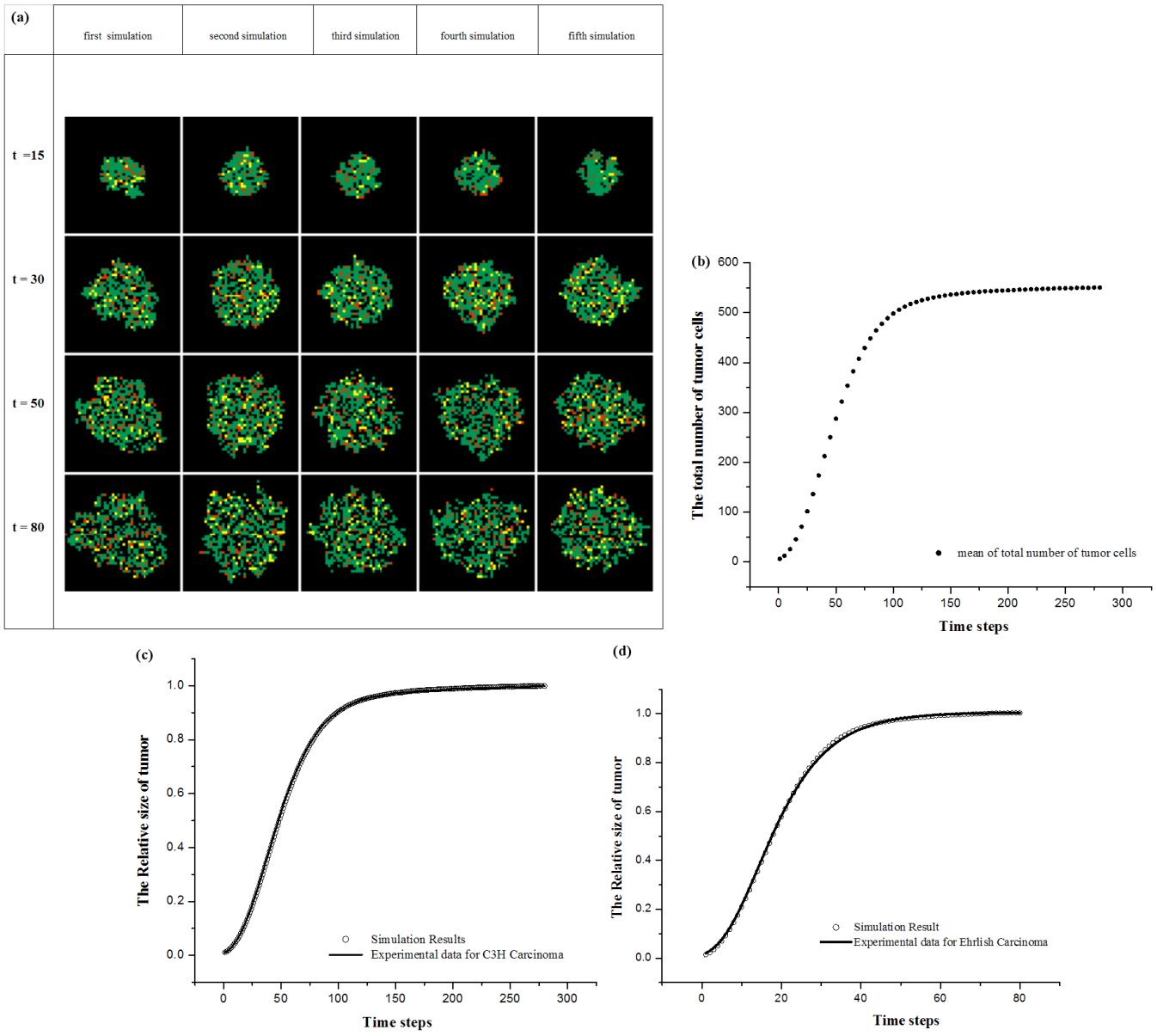


Fig. 6. (a) Influences of different series of pseudo-random numbers from five different seeds on the tumor shape on 47 × 47 square lattices with time progression for the same simulation settings as in Fig. 4(a). (b) Typical averaged growth curve, where the error bars are of the same magnitude as the size of the points. The simulation result is for an average over 1000 individual simulations with the parameters $r_{prolif.} = 0.25$, $r_{binding} = 0.04$, $r_{escape} = 0.6$, $r_{lysis} = 0.3$, $r_{decay} = 0.35$, and $K = 550$. (c) Comparison between the simulated tumor growth (circles) and the experimental growth curves *in vivo* for the spontaneous mouse carcinoma C3H (Steel [41] black solid line) with a coefficient of nonlinear regression $r^2 = 0.99985$. The Gompertz parameters are $V_o = 0.0376$ (cm)$^3$, $A = 0.177$ (day)$^{-1}$, $B = 0.0311$ (day)$^{-1}$, and $V_{max} = 11.12$ (cm)$^3$. The parameter settings are $r_{prolif.} = 0.25$, $r_{binding} = 0.04$, $r_{escape} = 0.6$, $r_{lysis} = 0.3$, $r_{decay} = 0.35$, and $K = 550$ with $N_o = 6.02$ and $N_{max} = 551.18$. (d) Comparison between the simulated tumor growth and the experimental growth curves *in vivo* for mouse Ehrlich [41] carcinoma with the coefficient of nonlinear regression $r^2 = 0.9997$. The Gompertz parameters are $V_o = 0.0226$ (cm)$^3$, $A = 0.456$ (day)$^{-1}$, $B = 0.102$ (day)$^{-1}$, and $V_{max} = 1.94$ (cm)$^3$. The parameter settings are $r_{prolif.} = 0.85$, $r_{binding} = 0.1$, $r_{escape} = 0.5$, $r_{lysis} = 0.35$, $r_{decay} = 0.35$, and $K = 550$ with $N_o = 8.381$ and $N_{max} = 627.379$.

as that of two-compartment cell-population model of Gyllenberg and Webb [31] also revealed Gompertzian growth.

## IV. COMPARISON OF SIMULATION RESULTS WITH EXPERIMENTAL RESULTS

A spatial visualization of tumor spreading on the two-dimensional square lattice leads us to some results: The growth curve from simulation in good agreement with experimental data for Ehrlich mouse carcinomas and for spontaneous mouse carcinomas (C3H) as reported by Steel [41]. The fractality of the boundary, the spatial distribution of cell proliferation, and the relevant biological implications will be represented.

### 1. Snapshots of Five Typical Simulated Tumors and the fractality of the boundary

The different morphologies of five typical simulated tumor patterns are shown in Fig. 6(a). Fig. 6(b) shows the growth curve for an average of over 1000 realizations.

The tumors obtained from the stochastic model are found to have an approximately circular shape with a rough boundary, as shown in Fig. 3(a). A few researchers [6–8,19,46–48] have been interested in the fractal dimension ($D_f$) of the stochastic growth model. We define the boundary cells of the simulated tumor using assuming that they are the outermost cells of the tumor in each row and each column in the lattice. The irregular boundaries of tumors can be examined by using a fractal geometric analysis. Moreover, the concept and measurement of fractal dimension by using the box-counting method is given by Bru *et al.* [20], Cross [49], Laird [50]. Malignant melanomas *in vivo* have been investigated and the fractal dimension of the boundary of the tumor is found to lie mainly in the range 1.05 – 1.30 [49]. Bru, *et al.* [20] and also published in vitro and *In-vivo* experimental data for the boundary of human and animal solid tumors with values of $D_f$ in the range of 1.09 – 1.34, which agrees well with the data of Cross [49]. Our mean fractal dimension of five tumor boundaries (between time steps 10 and 350) lies in 1.11 – 1.22, which agrees well with the observations of other researchers Bru *et al.* [20], Lefever and Erneux [23], and Cross [49]. The fluctuating boundary of a simulated tumor can be show to have nearly the same shape as the boundary of tumors in clinical studies.

### 2. Comparisons of the Average Growth Curve with the Experimental Data

The Gompertz growth curve is the most commonly used curve to fit the experimental data for *in-vivo* tumor growth [40,41,50,51] and is an important feature noticed in actual tumor growth. The Gompertz curve [41,52,53] is given as

$$V(t) = V_o \exp\left\{\frac{A}{B}(1-\exp(-Bt))\%\right\}, \qquad (1)$$

where $V(t)$ is the size of the tumor at time $t$, $V_o$ is the initial size, and $A$ and $B$ are two positive parameters whose values are determined by a least-square best fit of Eq. (1) to the data. Fig. 6(a) shows the average growth curve of a thousand tumors. At time $t$ tumor $i$ will give $N_i(t)$, with the error bar for $Ts$ tumors being defined as $2\sqrt{\frac{\sum_{i=1}^{Ts}(N_i(t)-\bar{N}(t))^2}{Ts-1}}$ at the 95 % confidence interval.

Fig. 6(b) represents the averaged growth curve from 1000 simulation runs with their error bars having the same magnitude as the data points. The averaged growth data from our simulation runs with settings $r_{prolif} = 0.25$, $r_{binding} = 0.04$, $r_{escape} = 0.6$, $r_{lysis} = 0.3$, $r_{decay} = 0.35$, and $K = 550$ is shown in Fig. 6(c). It is noteworthy to note that the Gompertz curve was used to fit the experimental growth curve of tumors *in vivo*. The Gompertz parameters for the experimental data for a spontaneous mouse carcinoma (C3H) are $V_o = 0.0376$ $(\text{cm})^3$, $A = 0.177$ $(\text{day})^{-1}$, $B = 0.0311(\text{day})^{-1}$, and $V_{max} = 11.12$ $(\text{cm})^3$. To obtain the fit, we had to normalize both the simulation and the experimental data. The normalization of the Gompertz curve was such that the maximum size and the normalization of the simulated data was, respectively, $N_o = 6.02$ and $N_{max} = 551.18$. The two normalized growth curves are shown together in Fig. 6(c).

The averaged growth curve yielded by our simulation runs with settings $r_{prolif} = 0.85$, $r_{binding} = 0.1$, $r_{escape} = 0.5$, $r_{lysis} = 0.5$, $r_{decay} = 0.5$, and $K = 550$ is shown in Fig. 6(d). The Gompertz parameters for the experimental data of Ehrlich carcinomas in mice are $V_o = 2.26 \times 10^{-7}$ $(\text{cm})^3$, $A = 0.456$ $\text{day}^{-1}$, $B = 0.102$ $\text{day}^{-1}$, and $V_{max} = 1.94$ $\text{cm}^3$. The normalization of the simulated data was such that $N_{max} = 625$ and $N_o = 8.394$. The two normalized growth curves for Ehrlich carcinomas are shown together in Fig. 6(d).

### 3. Spatial Distribution of proliferated Cell in tumors

Bru *et al.* [20], clinically studied the spatial distribution of cell proliferation in tumors by counting after tracking with Bromodeoxyridine (Brdu). In particular, Bru *et al.* [20] defined three regions of the avascular tumor on the basis of the radius of the tumor (assuming that the tumor is circular). The innermost region lies in the region $0 \le r_i < \text{R}/2$. The intermediate region lies in the region $\text{R}/2 \le r_i < 4\text{R}/5$. Finally, the outermost region lies in the region $r_i \ge 4\text{R}/5$. $r_i$ is the distance of a particular site occupied by a cancer cell from the center

of the tumor. They measured the number of proliferating cells in each of the three regions in a human colon adenocarcinoma. They found that the innermost region contained 6 % of the proliferating cancer cell and made up 25 % of the tumor. The intermediate region contained 14 % of the proliferating cells and made up 39 % of the tumor. The last region contained 80 % of the proliferating cells and made up 36 % of the tumor. Most of the proliferating cells were found in the outermost regime, similar to that found by Bru *et al.* [20]. The ratio of proliferating cancer cells found in the three regions is 80 : 14 : 6 (in order of outermost to innermost). Fig. 4(a) has shows the proliferating cells in a typical tumor. We measured these quantities by averaging over 1000 simulated tumors with parameters $r_{prolif} = 0.85$, $r_{binding} = 0.1$, $r_{escape} = 0.5$, $r_{lysis} = 0.35$, $r_{decay} = 0.35$, and $K = 550$. We empirically set the saturation phase of the tumor growth from time steps 80 to 150 and the ratio of proliferating tumor cells that we found for the outermost, intermediate, and innermost regimes, was 71 : 17 : 11. The errors were 0.094, 0.082, and 0.124, respectively. We may conclude that the proliferating cells of the simulated tumor were located mostly in the outermost regions.

### 4. Sensitivity Analysis by Varying parameters with Some Biological Effect

We changed the values of some of the parameters in the model to see how the growth of the tumor would be affected. The ranges chosen for the parameter values in our model were motivated either by experimental clinical data [1, 23] or by the computational experiment results Steel [41], and Barabasi and Stanley [51]. All simulation results could be fitted well with a Gompertz function.

Mathematically, the behavior of the Gompertz curve can be divided into three regions [53]. These are determined by the position of the inflection point [41], and the crossover time [51]. Biologically speaking, the three regions reflect different growth behavior. The first region or early phase reflects the dynamics of the initial stage of tumorigenesis. The phase continues until the number of tumor cells reaches a value equal to 0.37 of the maximum number of tumor cells. The time step at which this occurs is called the infection point in the curve. We denote this time as $t_1$. The second region or intermediate phase of the growth curve is the portion of the curve which begins at $t_1$ and extends to the crossover point at $t_2$. The crossover point is the intersection of the tangent lines of the initial portion of the Gompertz curve and of the saturated part of the Gompertz curve. Then, the time $t_2$ means the time to reach the saturated phase of the Gompertz curve. The third region of the curve starts at the cross over point and extends into the saturated state. The three regions of the Gompertz curve are shown in Appendix B.

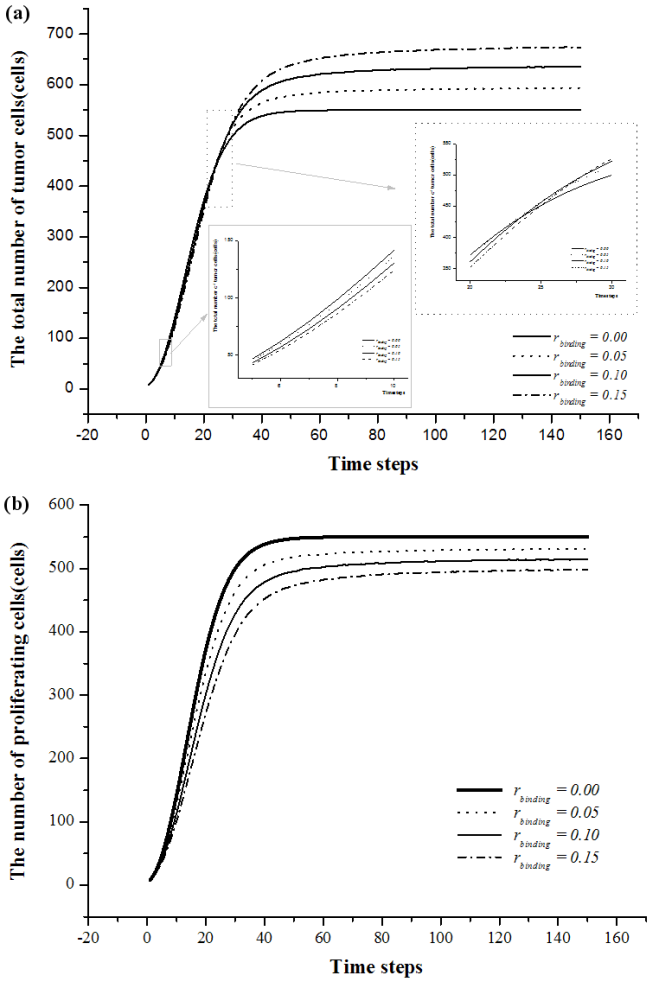


Fig. 7. (a) Plots of the time evolution of the total numbers of tumor cells. The inset shows magnified time step of 5 to 10 and 20 to 30. The simulation results are averaged over 1000 individual realizations by varying the value of $r_{binding}$ from 0.00 to 0.15 in steps of 0.05 while fixing the other values at $r_{prolif.} = 0.85$, $r_{escape} = 0.5$, $r_{lysis} = 0.35$, $r_{decay} = 0.35$, and $K = 550$. (b) Plots of the time evolutions of the numbers of proliferating cells. The simulation results are averaged over 1000 individual realizations with the same parameters as in Fig. 7(a).

To see how the immune system influences the growth of the tumor, we varied $r_{binding}$ and $r_{escape}$ because the value of these two rates depends on the immune system. We varied the value of $r_{binding}$ and obtained the simulation results as shown in Figs. 7(a), and 7(b). We can conclude that the proliferating cells decrease as the rate of binding with TICLs increases. This also causes saturation to be reached at a later time.

The escape rate reflects the efficiency of cancer cells evading the binding process of TICLs. A greater escape rate indicates a shorter time for binding maintenance before cancer cells evade unfolding TICLs. We varied $r_{escape}$ to get the simulation results shown in Figs. 8(a),

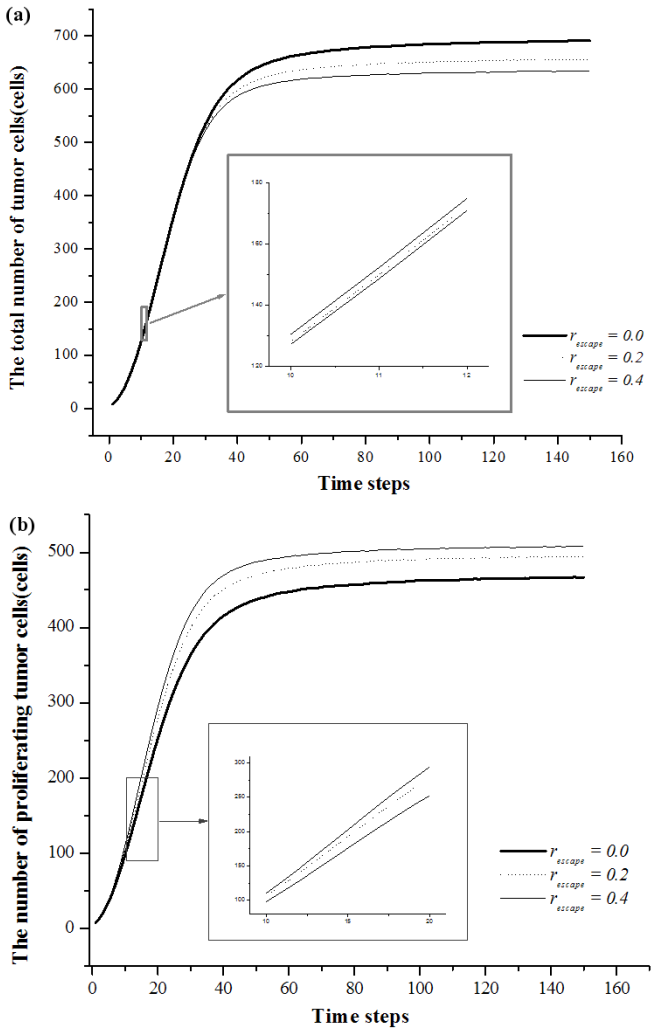


Fig. 8. (a) Plots of the time evolution of the total number of tumor cells. The simulation results are averaged over 1000 individual realizations by varying the value of $r_{escape}$ from 0.0 to 0.4 in steps of 0.2 while fixing the other values at $r_{prolif.} = 0.85$, $r_{binding} = 0.1$, $r_{lysis} = 0.35$, $r_{decay} = 0.35$, and $K = 550$. (b) Plots of the time evolutions of the total number and the number of proliferating tumor cells of the simulated tumor. The simulation results are averaged over 1000 individual realizations with the same parameters as in Fig. 8(a).

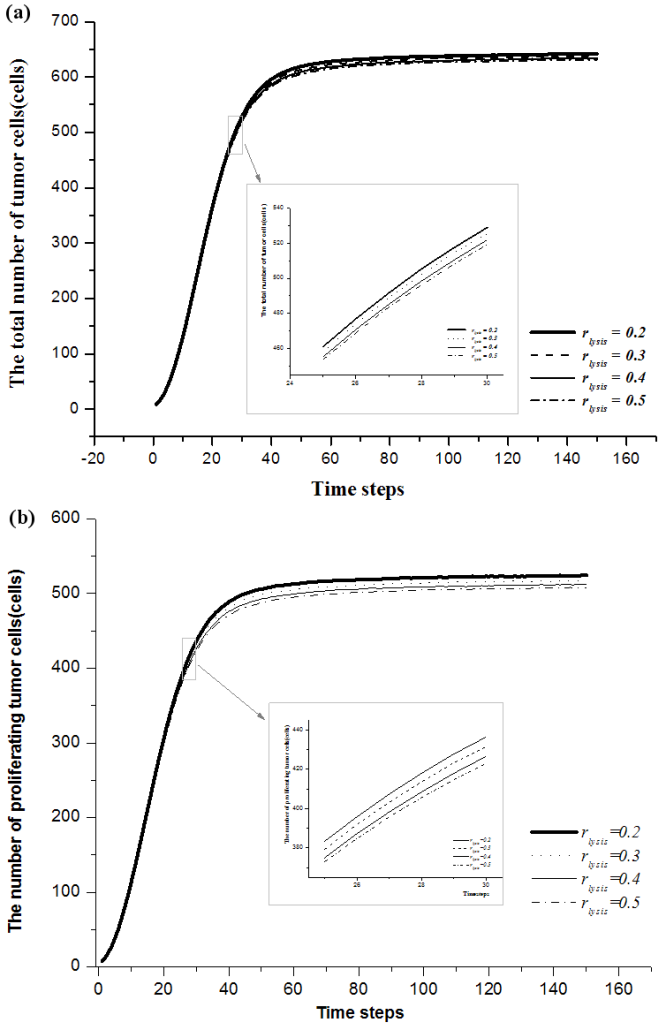


Fig. 9. (a) Plots of the time evolution of the total number of tumor cells. The simulation results are averaged over 1000 individual realizations by varying the value of $r_{lysis}$ while fixing the other values at $r_{prolif.} = 0.85$, $r_{binding} = 0.1$, $r_{escape} = 0.5$, $r_{decay} = 0.35$, and $K = 550$. (b) Plots of the time evolutions of the total number and the number of proliferating tumor cells of the simulated tumor. The simulation results are averaged over 1000 individual realizations with the same parameters as in Fig. 9(a).

and 8(b). The growth curves for the proliferating tumor cells show that increasing $r_{escape}$ will cause a rate of growth increase in the initial phase. Saturation will be achieved in a shorter time with a greater tumor size as $r_{escape}$ increases.

The lysis rate, $r_{lysis}$, is the death rate of cancer cells due to programmed death. We varied the value of the parameter $r_{lysis}$ and obtained the results shown in Fig. 9(a) and 9(b). The growth of the number of proliferating tumor cells increases only slightly with increasing $r_{lysis}$ in the initial phase. The growth curves reach crossover more they do for than smaller sizes. We found an essential difference concerning variation of the lysis rate between our model and that of Qi *et al.* [1]. The conclusion of Qi *et al.* [1] is that a greater $r_{lysis}$, gives a greater number of proliferating cells in the third region. We can get the same result as Qi *et al.* do [1] without the escape mechanism.

The decay rate, $r_{decay}$, may be considered as the efficiency of TICLs in destroying the cancer cells with programming for lysis after unfolding. A greater decay rate yields a shorter time for destruction of cancer cells. $r_{decay}$ was varied from 0.2 to 0.5 in steps of 0.1 with

the values of all the other parameters kept constant. Increasing the decay rate of the cancer cells resulted in a decrease in the total number of cancer cells and a slight increase in the number of proliferating tumor cells in the third region. The crossover point for each curve was be reached in a shorter time.

From our studies, it is yet to be seen if experimentalists can take advantage of our findings. After we have the simulational results for various parameters, it is worth discussing some biological implications of those results so that the biological impacts for some parameters might be understood. The biological meaning of each parameter is as follows:

1. The proliferative activity of tumor cells is reduced by decreasing $r_{prolif.}$ Clinical trials have shown that increasing proliferation rates yield smaller tumors [31,54]. For instance, Blay *et al.* [54] studied gastrointestinal stromal tumors (GIST), which are solid tumors. GISTs exhibit typical activating mutations of KIT or PDGFRA proto-oncogene, which are most likely causal molecular events of GISTs. Oncogene-targeted therapy using Imatinib, a tyrosine kinase inhibitor blocking most mutated-activated KIT and (platelet-derived growth-factor receptor) PDGFR $\alpha$ proteins of GISTs, controlled tumor growth up to 85 %. This therapy may lead to elimination of both new proliferating tumors and existing tumors. The parameters that affect adoptive therapy may decrease $r_{prolif.}$, and the comparison with our simulation results is good.

2. Ehe defensive activity of immune cells is modified by increasing $r_{binding}$ and $r_{lysis}$ in order to have a faster response by the immune response system. Studying the many clinical experiments (1995-2001) of Matzavinos and Chaplain [11], we conclude that cytokines are one of the components of the immune system that are involved in modulating the local cellular immune response dynamics with the production of several interleukins (IL-2, IL-10, and IL-12), cell-adhesion molecules and chemokines in tumor tissue, the induced chemotaxis of T-cells, and the cytotoxic reactions of TICLs against tumor cells. Consequently, the effectiveness of cytokines might be the reason for increasing $r_{binding}$ and $r_{lysis}$ in the kinetic model.

3. A modification of the aggressiveness of immune cells against the tumor by increasing the parameter $r_{lysis}$ give a more efficient immune activity. Almost all breast cancer patients have hormone receptor positivity. Tamoxifen is a hormonal treatment for breast cancer. Hickman [55] has studied anticancer therapies by induced apoptosis. Ellis *et al.* [56] have reported clinical studies that show that increases in apoptosis in human breast cancer occur with tamoxifen treatment. Dowsett *et al.* [39,57], Cameron *et al.* [40], and Bardon *et al.* [58] studied tumor regression in breast cancer xenografts with tamoxifen and have been reported the same results. Xenograft studies support increased apoptosis and decreased proliferation after oestrogen withdrawal [39]. However, the relative importance of these two processes still remains unclear [40].

We increased $r_{lysis}$ with the other parameters fixed, which means that the escape parameter is also fixed. The kinetic model in Fig. 1 shows the competition between TICLs and cancer cells. Increasing $r_{lysis}$ and fixing $r_{escape}$ may yield enhanced immune efficiency, implying a decrease in the number of proliferating cells due to the escape process. If the rate $r_{lysis}$, is increased the dead cancer cells increase in number, which also decreases the quantity of escaping cancer cells from the TICL-cancer cell complexes, ultimately decreasing proliferation.

## V. CONCLUDING REMARKS

The kinetic model shown in Fig. 1 shows a tumor growth that is governed by the processes of proliferation, binding, escape, lysis, and decay by using the cellular automaton method with five parameters to represent these processes. With this kinetic model and the simulation method, we can show that different sets of the five kinetic parameters will give differing Gompertzian curves.

We can conclude from the simulation results that a greater tumor size might not indicate aggressiveness of tumor growth. In particular, we agree with Steel [41] that the quantity of proliferating cells be a better indication of tumor size.

This CA model also allows us to quantify the proportion of each cell type within a simulated tumor as a function of each set of five parameters. The cellular automata model on a three-dimensional square lattice is also in the process of development.

## APPENDIX A: FLOWCHART OF THE MONTE CARLO CELLULAR AUTOMATA ALGORITHM OF TUMOR

Initial Configuration : with five proliferating tumor cells in the middle of the tissue model

## APPENDIX B

Plots of the time evolution of the total number of tumor cells (circles). The three segments of the sigmoidal Gompertzian curve from the simulation results show

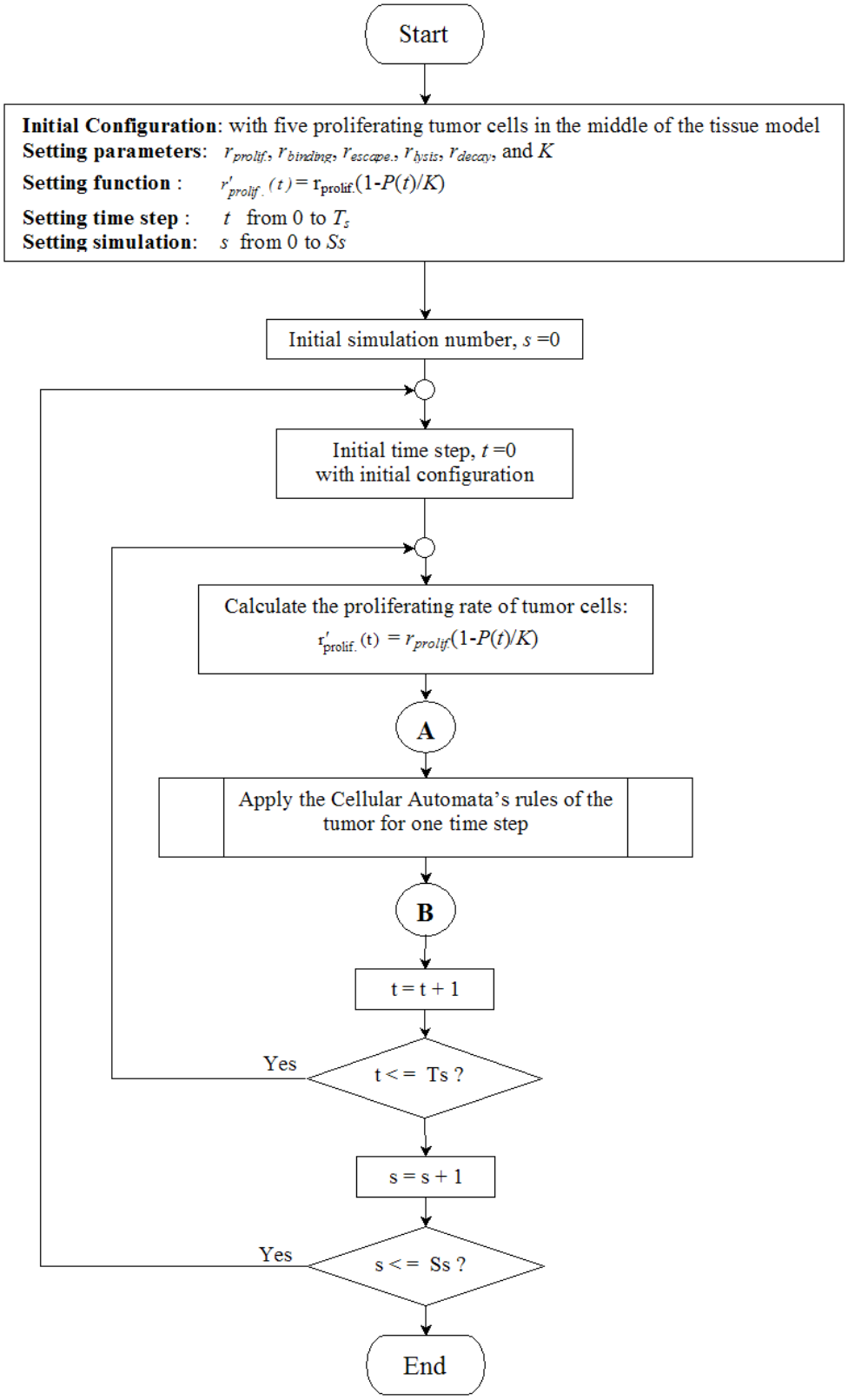
Start
**Initial Configuration**: with five proliferating tumor cells in the middle of the tissue model
**Setting parameters**: $r_{prolif.}$, $r_{binding}$, $r_{escape.}$, $r_{lysis}$, $r_{decay}$, and $K$
**Setting function** : $r'_{prolif.}(t) = r_{prolif.}(1\text{-}P(t)/K)$
**Setting time step** : $t$ from 0 to $T_s$
**Setting simulation**: $s$ from 0 to $Ss$
Initial simulation number, $s$ =0
Initial time step, $t$ =0 with initial configuration
Calculate the proliferating rate of tumor cells: $r'_{prolif.}(t) = r_{prolif}(1\text{-}P(t)/K)$
A
Apply the Cellular Automata's rules of the tumor for one time step
B
t = t + 1
Yes
t <= Ts ?
s = s + 1
Yes
s <= Ss ?
End

The algorithm of cellular automata 's rule apply for a time step

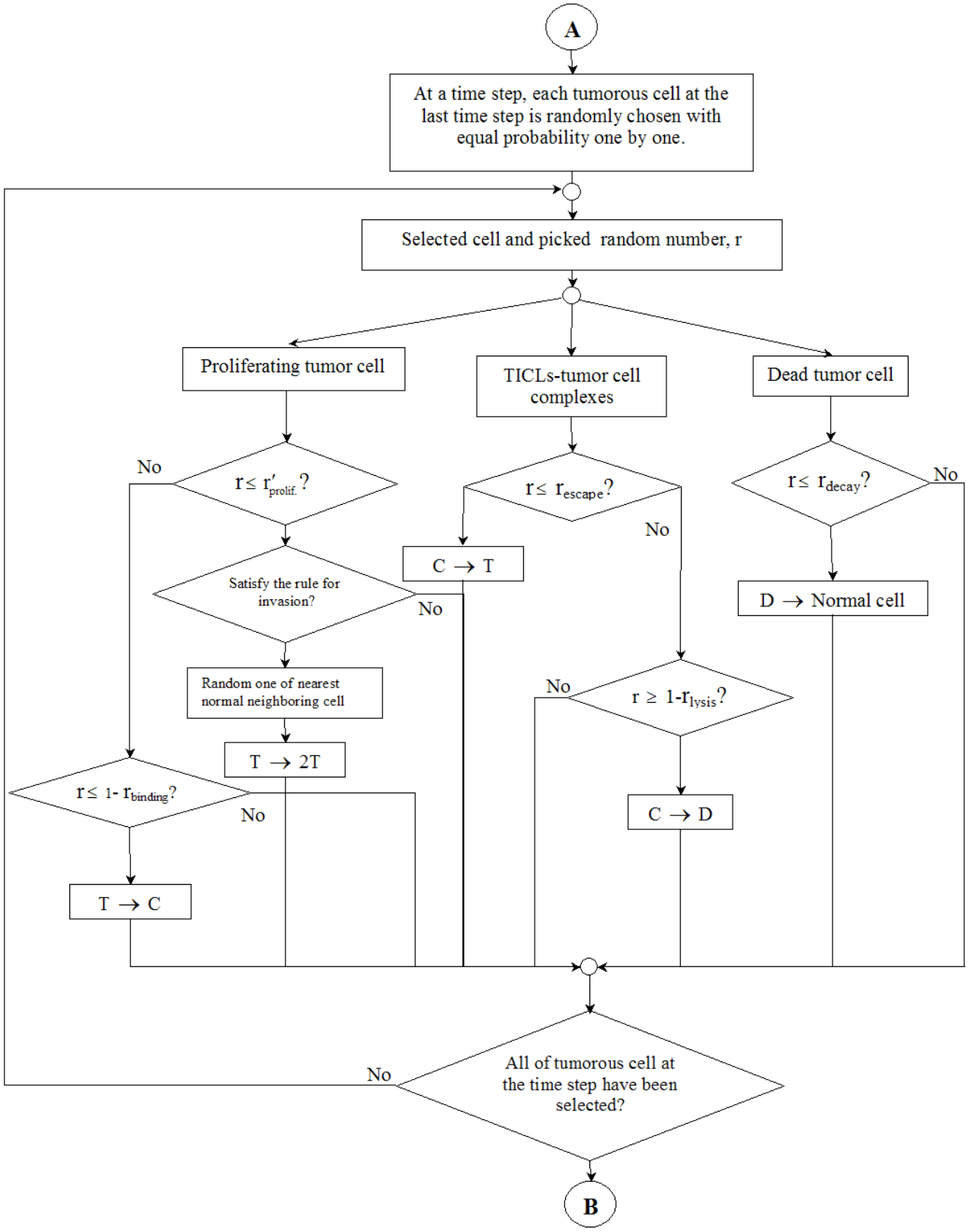

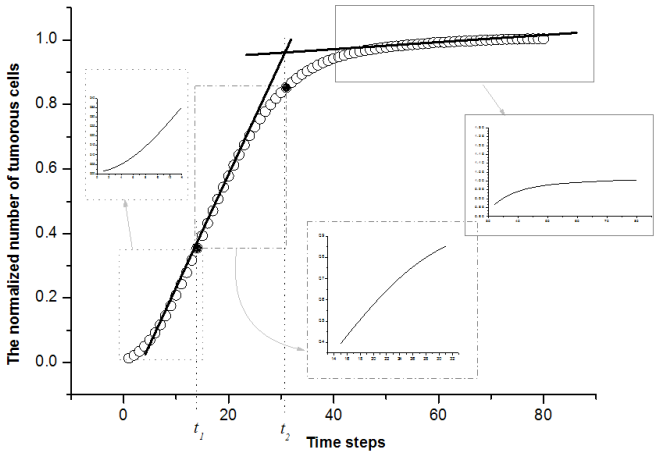


different growth dynamics. The first segment has range from 0 to $14(t_1)$ time steps at the first solid circle; the second phase runs from day 15 until the time step at $31(t_2)$, that is the crossover time; the third phase begins at 32 days from the second solid circle. The simulation results are averaged over 1000 individual realizations with the simulation settings $r_{prolif.} = 0.85$, $r_{binding} = 0.1$, $r_{escape} = 0.5$, $r_{lysis} = 0.35$, $r_{decay} = 0.35$, and $K = 550$.

## ACKNOWLEDGMENTS

The authors would like to thank J. Poulter for his fruitful discussions and proofreading. One of the authors (A. B.) would like to thank T. J. Newman and the Department of Physics and Astronomy at Arizona State University for the training program in the US for one year (2003-2004), C. Quince who helped in improving programme development. T. Dhirasakdanon, and T. Sungkaworn who supplied relevant important papers. Additionally, we would like to thanke P. Kanthang, W. Ngamsa-ad, S. Chadsuthi, H. Pitakjakpipop, and C. Modchang who are in the biophysics group at Mahidol University, for their technical assistance with software support concerning.This research work was financially supported in part by Mahidol University, the Thailand Research Fund (TRF), the National Center for Engineering and Biotechnology, Thailand (BIOTEC), and the Institute of Innovation and Development of Learning Process.

## REFERENCES

[1] A. S. Qi, X. Zheng, C. Y. Du and B. S. An, J. Ttheor. Biol. **161**, 1 (1993).
[2] A. R. Kansal, S. Torquato, G. R. Harsh, E. A. Chiocca and T. S Deisboeck, J. Theor. Biol. **203**, 367 (2000).
[3] A. R. Kansal, S. Torquato, G. R. Harsh, E. A. Chiocca and T. S Deisboeck, Biosystems. **55**, 119 (2000).
[4] J. Smolle and H. Stettner, J. Theor. Biol. **161**, 63 (1993).
[5] D. Kirschner and J. C. Panetta, J. Math. Bio. **37**, 235 (1998).
[6] Jr. S. C. Ferreira, M. L. Martins and M. J. Vilela, Physica A **261**, 569 (1998).
[7] Jr. S. C. Ferreira, M. L. Martins and M. J. Vilela, Physica A **271**, 245 (1999).
[8] M. V. Voitikova, arXiv:comp-gas/9811001, (1998).
[9] J. Smolle, H. P. Soyer, F. M. Smolle-Juettner, H. Stettner and H. Kerl, Path. Res. Pract. **186**, 467 (1990).
[10] A. Matzavinos and J. Chaplain, Math. Med. and Bio. **21**, 1 (2004).
[11] A. Matzavinos and J. Chaplain, C. R. Biologies. **327**, 995 (2004).
[12] W. Duchting and T. Vogelsaenger, Int. J. Bio-Medical Computing **12**, 377 (1981).
[13] N. Bellomo and L. Preziosi, Mathl. Comput. Modelling **32**, 413 (2000).
[14] M. Galach, Int. J. Appl. Math. Comput. Sci. **13**, 395 (2003).
[15] T. Alarcon, H. M. Byrne and P. K. Maini, J. Theor. Biol. **225**, 257 (2003).
[16] N. Buric and D. Todorovic, Chaos, Solitons and Fractals **13**, 645 (2002).
[17] P. Daugulis, *et al.*, *Hopf bifurcation analysis for angiogenesis models, Discrete and Continuous Dynamical Systems*, in press.
[18] S. Habib, C. Molina-Paris and T. S Deisboeck, Phys. A **327**, 501 (2003).
[19] Y. Mansury and T. S. Deisboeck, Physica A **219**, 219 (2004).
[20] A. Bru, S. Albertos, J. L. Subiza and J. L. Garcia-Asenjo, Biophysic Journal. **85**, 2948 (2003).
[21] V. A. Kuznetsonov and M. A. Taylor, Bull. Math. Biol. **56**, 295 (1994).
[22] G. J. Pettet, C. P. Please, M. J. Tindall and D. L. McElwain, Bull. Math. Biol. **63**, 231 (2001).
[23] R. Lefever and T. Erneux, *Plenum Publishing Corporation* (New York, 1984).
[24] A. A. Patel, E. T. Gawlinski, S. K. Lemieux and R. A. Gatenby, J. Theor. Biol. **213**, 315 (2001).
[25] A. Bru, S. Albertos, J. L. Subiza and J. L. Garcia-Asenjo, Phys. Rev. Lett. 92 **23**, 238101 (2004).
[26] M. R. Owen and J. A. Sherratt, J. Theor. Biol. **189**, 63 (1997).
[27] R. B. Conolly and J. S. Kimbell, Toxicology and Applied Pharmacology **124**, 284 (1994).
[28] D. D. Dionysiou, G. S. Stamatakos, N. K. Uzunoglu and K. S. Nikita, Comp. in Bilol., Med. Article in press (2005).
[29] D. Drasdo, R. Kree and J. S. McCaskill, Phys. Rev. E **52**, 6635 (1995).
[30] H. P. Greenspan, J. Theor. Biol. **56**, 229 (1976).
[31] M. Gyllenberg and G. F. Webb, Growth, Dev. Aging **53**, 25 (1989).
[32] W. Sa-Nguansin, W. Triampo and N. Nattavut, J. Korean Phys. Soc. **46**, 1429 (2005).
[33] J. Wong-ekkabut, W. Triampo, D. Triampo, I. M. Tang and Y. Lenbury, J. Korean Phys. Soc. **45**, 310 (2004).
[34] A. Kataki, P. Scheid, M. Piet, B. Marie, N. Martinet, Y. Martinet and J.-M. Vignaud, J. Lab Clin. Med. **140**,

320 (2002).
[35] A. S. Perelson and G. I. Bell, J. Immunol. **129**, 2796 (1982).
[36] A. S. Perelson, L. S. Mackoos and B. Bonavida, V. Kinetics of (1984).
[37] S. Jain, Cancer Cell Int. **2**, 13 (2002).
[38] G. C. Easty, G. C. Ambrose and F. J. Croe (Eltis Horwood Limited, 1975), p. 58.
[39] M. Dowsett, C. Archer, L. Assersohn, R. K. Gregory, P. A. Ellis, J. Salter, J. Chang, P. Mainwaring, I. Boeddinghaus, S. R. D. Johnston, T. J. Powles and I. E. Smith, Endocrine-Related **6**, 25 (1999).
[40] D. A. Cameron, A. A. Ritchie and W. R. Miller, Eur. J. Can. **37**, 1545 (2001).
[41] G. G. Steel (Clarendon press, New York, 1977).
[42] A. Bru, J. M. Paster, I. Fernaud, I. Bru, S. Melle, C. Berenguer, Phys. Rev. Lett. **81**, 4008 (1998).
[43] L. P. Preziosi, J. Immunol. **132**, 2190 (2003).
[44] A. Anichini, G. Bevila cqua, R. Gavazzi and P. L. Lollini, Eds. (1995).
[45] F. Kozusko and Z. Bajzer, Math. Bios. **185**, 153 (2003).
[46] P. F. Ho and C. Y. Wang, Math. Biosci. **155**, 139 (1999).
[47] S. Dormann, The Dessertation Zur Erlangung des Grades eines Doktors der Naturwissenschaften (2000).
[48] C. Y. Wang and J. Bassingthwaighte, Math. Bio. **142**, 91 (1997).
[49] S. S. Cross, J. Pathol. **182**, 1 (1997),
[50] A. K. Laird, Br. J. Cancer **19**, 278 (1964).
[51] A. L. Barabasi and H. Stanley (Cambridge University Press, Cambridge, 1995).
[52] W. Mueller-Klieser, S. Schreiber-Klais, S. Walenta and M. H. Kreuter, Int. J. Oncol. **21**, 1307 (2002).
[53] L. Norton, R. Simon, H. D. Brereton and A. E. Bogden, Nature **264**, 542 (1976).
[54] J.-Y. Blay, S. Bonvalot, P. Casali, H. Choi, M. Debiec-Richter, A. P. Dei-Tos, J.-F. Emile, A. Gronchi, P. C. W. Hogendoorn, H. Joensuu, C. A. Le, M. J. Mac-Clure, J. Maurel, N. Nupponen, I. Ray-Coquard, P. Reichardt, R. Sciot, S. Stroobants, M. van Glabbeke and G. D. Demetri, Annals of Oncology **16**, 566 (2005).
[55] J. A. Hickman, Cancer Metastasis Rev. **11**, 121 (1992).
[56] P. A. Ellis, G. Saccani Jotti, R. Clarke, S. R. D. Johnston, E. Anderson, A. Howell, R. A'Hern, J. M. Salter, S. Detre, R. Nicholson, J. Robertson, M. Baum, I. E. Smith and M. Dowsett, International Journal of Cancer **72**, 608 (1997).
[57] M. Dowsett, S. R. D. Johnston, J. Newby, M. Golding, N. Sacks and I. E. Smith, Endoc-Relat Cancer **2**, 3 (1995).
[58] S. Bardon, F. Vignon, P. Montcourrier and H. Rochefort, Cancer Res. **47**, 1441 (1987).
[59] D. A. Cameron, A. A. Ritchie, S. Langdon, T. J. Anderson and W. R. Miller, Breast Cancer Research and Treatment **45**, 99 (1977).
[60] P. Waliszewski and J. Konarski, Chaos, Solitons and Fractals **16**, 665 (2002).